

Spatial coherence measurements of a 13.2 nm transient nickel-like cadmium soft X-ray laser pumped at grazing incidence

Y. Liu¹, Y. Wang², M. A. Larotonda², B. M. Luther², J. J. Rocca², and D. T. Attwood¹

¹NSF ERC for Extreme Ultraviolet Science and Technology and College of Engineering, University of California at Berkeley, and Center for X-ray Optics, Lawrence Berkeley National Laboratory, Berkeley, CA 94720
ywliu@lbl.gov

²NSF ERC for Extreme Ultraviolet Science and Technology and Department of Electrical and Computer Engineering, Colorado State University, Fort Collins, CO 80523

Abstract: The spatial coherence of a 13.2 nm transient collisional Ni-like Cd soft X-ray laser pumped at 23 degrees grazing incidence was measured in a series of Young's double-slit experiments. We observed pronounced fringe visibility variations associated with microstructures in the beam's intensity profile. The transverse coherence length was measured to be about 1/20 of the beam diameter and did not significantly improve with longer plasma columns. The equivalent incoherent source size is determined to be 10 μm and the laser's peak spectral brightness $\sim 3 \times 10^{23}$ photons/sec/mm²/mrad² within less than 0.01% spectral bandwidth.

©2006 Optical Society of America

OCIS codes: (140.7240) UV, XUV, and X-ray lasers; (030.1640) Coherence and Statistical optics; (340.7440) X-ray optics: X-ray imaging

References and links

1. Y. Wang, M. A. Larotonda, B. M. Luther, D. Alessi, M. Berrill, V. N. Shlyaptsev, and J. J. Rocca, "Demonstration of high-repetition-rate tabletop soft-x-ray lasers with saturated output at wavelengths down to 13.9 nm and gain down to 10.9 nm," *Phys. Rev. A* **72**, 053807 (2005).
2. H. C. Kapteyn, M. M. Murnane and I. P. Christov, "Extreme Nonlinear Optics: Coherent X Rays from Lasers," *Phys. Today*, **58**, 39-44 (2005).
3. K. A. Goldberg, P. Naulleau, P. Denham, S. B. Rekawa, K. Jackson, E. H. Anderson and J. A. Liddle, "At-wavelength alignment and testing of the 0.3 NA MET optics," *J. Vac. Sci. Tech. B* **22**, 2956-2961 (2004).
4. P. P. Naulleau, "Advanced EUV Lithography capabilities at Lawrence Berkeley National Laboratory's Advanced Light Source," Proceedings, SEMI Technology Symposium 2004.
5. P. P. Naulleau, K. A. Goldberg, E. H. Anderson, P. Denham, B. Hoef, K. Jackson, A. Morlens, and S. Rekawa, "EUV microexposures at the ALS using the 0.3-NA MET projection optics," *Microolithography 2005*, paper [5751-04], i.b. *Proc. SPIE* **5374**, 881-891 (2004).
6. Y. Liu, A. Barty, E. Gullikson, J. S. Taylor, J. A. Liddle, and O. Wood, "A dual-mode actinic EUV mask inspection tool," in *Emerging Lithographic Technologies IX*, R. Scott Mackay, ed., *Proc. SPIE* **5751**, 660-669 (2005).
7. W. Chao, B. D. Harteneck, J. A. Liddle, E. H. Anderson, and D. T. Attwood, "Soft X-ray microscopy at a spatial resolution better than 15 nm," *Nature* **435**, 1210 (2005).
8. G. Vaschenko, C. Brewer, F. Brizuela, Y. Wang, M. A. Larotonda, B. M. Luther, M. C. Marconi, J. J. Rocca, C. S. Menoni, E. H. Anderson, W. Chao, B. D. Harteneck, J. A. Liddle, Y. Liu, D. T. Attwood, "Sub-38 nm resolution tabletop microscopy with 13 nm wavelength laser light," *Opt. Lett.* **31**, 1214-1216 (2006).
9. J. J. Rocca, Y. Wang, M. A. Larotonda, B. M. Luther, M. Berrill, and D. Alessi, "Saturated 13.2 nm high-repetition-rate laser in nickellike cadmium", *Opt. Lett.* **30**, 2581-2583 (2005).
10. R. Keenan, J. Dunn, P. K. Patel, D. F. Price, R. F. Smith, and V. N. Shlyaptsev, "High-repetition-rate grazing-incidence pumped x-ray laser operating at 18.9 nm," *Phys. Rev. Lett.* **94**, 103901 (2005).
11. B. M. Luther, Y. Wang, M. A. Larotonda, D. Alessi, M. Berrill, M. C. Marconi, J. J. Rocca, and V. N. Shlyaptsev, "Saturated high-repetition-rate 18.9-nm tabletop laser in nickellike molybdenum," *Opt. Lett.* **30**, 165-167 (2005).
12. R. A. London, "Beam optics of exploding foil plasma x-ray lasers," *Phys. Fluids* **31**, 184 (1988).
13. H. Tang, H. Daido, M. Kishimoto, K. Sukegawa, R. Tai, S. Mosesson, M. Tanaka, P. Lu, T. Kawachi, K. Nagashima, K. Nagai, T. Norimatsu, K. Murai, H. Takenaka, Y. Kato, K. Mima, K. Nishihara, "Spatial

- coherence measurement of 13.9 nm Ni-like Ag soft x-ray laser pumped by a 1.5 ps, 20 J Laser," Jpn. J. Appl. Phys. **42**, 443-448 (2003).
14. A. Lucianetti, K. A. Janulewicz, R. Kroemer, G. Priebe, J. Tümmeler, W. Sandner, P. V. Nickles, and V. I. Redkorechev, "Transverse spatial coherence of a transient nickel like silver soft-x-ray laser pumped by a single picosecond laser pulse," Opt. Lett. **29**, 881-883 (2004).
 15. M. Born and E. Wolf, *Principles of Optics, 7th Edition* (Cambridge University Press, 1999)
 16. R. A. London, M. Strauss and M. D. Rosen, "Modal analysis of x-ray laser coherence," Phys. Rev. Lett. **65**, 563-566 (1990).
 17. D. Attwood, *Soft X-rays and Extreme Ultraviolet Radiation: Principles and Applications* (Cambridge University Press, 1999)
 18. M. A. Larotonda, Y. Wang, M. Berrill, B. M. Luther, and J. J. Rocca, M. M. Shakya, S. Gilbertson, and Z. Chang, "Pulse duration measurements of grazing incidence pumped high repetition rate Ni-like Ag and Cd transient soft x-ray lasers," Opt. Lett., (2006), In press
 19. A. Klisnick, O. Guilbaud, D. Ros, K. Cassou, S. Kazamias, G. Jamelot, J.-C. Lagron, D. Joyeux, D. Phalippou, Y. Lechantre, M. Edwards, P. Mistry, and G. J. Tallents, "Experimental study of the temporal coherence and spectral profile of the 13.9nm transient X-ray laser," J. Quant. Spectrosc. Radiat. Transf. **99**, 370-380 (2006)
 20. O. Guilbaud, A. Klisnick, K. Cassou, S. Kazamias, D. Ros, G. Jamelot, D. Joyeux, and D. Phalippou, "Origin of microstructures in picosecond X-ray laser beams," Europhys. Lett. **74**, 823-829, (2006)
 21. P. D. Gasparyan, F. A. Starikov and A. N. Starostin, "Angular divergence and spatial coherence of X-ray laser radiation," Phys. Usp. **41**, 761-792 (1998).
 22. Y. Liu, M. Seminario, F. G. Tomasel, C. Chang, J. J. Rocca, and D. T. Attwood, "Achievement of essentially full spatial coherence in a high-average-power soft-x-ray laser," Phys. Rev. A **63**, 033802 (2001).
 23. P. Amendt, M. Strauss, and R. A. London, "Plasma fluctuations and x-ray laser transverse coherence," Phys. Rev. A. **53**, R23-R26 (1996).
 24. M. Nishikino, M. Tanaka, K. Nagashima, M. Kishimoto, M. Kado, T. Kawachi, K. Sukegawa, Y. Ochi, N. Hasegawa, and Y. Kato, "Demonstration of a soft-x-ray laser at 13.9 nm with full spatial coherence," Phys. Rev. A **68**, 061802 (2003).
 25. Y. Wang, E. Granados, M. A. Larotonda, M. Berrill, B. M. Luther, D. Patel, C. S. Menoni and J. J. Rocca, "High brightness injection seeded soft x-ray laser amplifier using a solid target," Phys. Rev. Lett. **97**, 123901 (2006).

1. Introduction

Recently there have been significant advances in the development of compact high repetition rate coherent sources at extreme ultraviolet (EUV) and soft x-ray (SXR) wavelengths. Two approaches are transient EUV/SXR lasers pumped by picosecond optical lasers [1] and high-order harmonic generation [2] from intense femtosecond lasers. In particular, significant research efforts have been directed towards the development of compact sources emitting at wavelengths close to 13.5 nm, where the next generation EUV lithography (EUVL) for fabricating semiconductor chips with feature size of 32 nm and smaller is planned. These sources would make it possible to perform at-wavelength inspection and metrology of EUVL optics on a laboratory scale, instead of using synchrotron radiation facilities as they are now [3-5]. Compared with other available EUV sources, EUV lasers have very narrow spectral bandwidth ($\Delta\lambda/\lambda$ typically in the order of 10^{-4}), thus making them ideal sources for applications such as at-wavelength wavefront interferometry [3] and high spatial resolution imaging using Fresnel zone-plates [6,7]. For these potential applications, the spatial coherence property of the beam plays a critical role. A high degree of spatial coherence is desired for interference-based applications, as in interferometry. On the other hand, spatial coherence must be controlled to achieve the ultimate spatial resolution in microscopy [6].

Recently table-top high repetition rate lasers operating in the vicinity of 13.5 nm have been demonstrated to produce average powers in excess of 1 μ J [1, 8]. The lasers, which operate on the 13.2 nm line of Ni-like Cd and the 13.9 nm line of Ni-like Ag, are excited by heating a pre-created plasma with a 6-8 ps optical laser pulse impinging at grazing incidence. This pumping geometry takes advantage of refraction of the pump beam in the plasma to increase the fraction of the pump energy absorbed in the gain region as compared to the conventional normal incidence pumping geometry [9,10]. Refraction has the advantage that it allows one to define the electron density at which the pump energy is absorbed based on only two parameters, the grazing incidence angle θ and the laser pump wavelength: $\theta = (n_e / n_{cp})^{1/2}$ [8-10], where n_e is the maximum electron density within the amplification region and n_{cp} is

the critical density at the wavelength of the pump. Hence when the grazing angle is changed, different parts of the density profile formed by the pre-pulse are preferentially heated. At a selected incidence angle of 23 degrees and an incident wavelength of 800 nm, the pump energy is most efficiently coupled in the region where the electron density is $n_e = 2.6 \times 10^{20} \text{ cm}^{-3}$, where large amplification can be obtained in transitions of Ni-like ions with wavelengths near 13.5 nm. This in turn significantly decreases the pump pulse energy required to operate the lasers in the gain saturated regime, allowing their operation at table-top scale and at increased repetition rate.

Several measurements of the spatial coherence of soft x-ray lasers excited using the conventional normal incidence geometry have been reported in the literature [12, 13]. It is of interest to study the coherence of soft x-ray lasers pumped at grazing incidence. Here we discuss the measurement of the spatial coherence of a 13.2 nm transient Ni-like Cd laser pumped at grazing incidence using classical Young's double-slit interference experiments. In the experiments we used a series of double-slits with different separations, which characterize the transverse coherence length. We also investigated the coherence with different plasma lengths. Similar experiments have been done with a 13.9 nm Ni-like Ag laser pumped at normal incidence [13]. Although 13.2 nm and 13.9 nm are both close to the 13.5 nm peak wavelength of standard Mo/Si multilayer coatings used in EUVL, the unsymmetrical shape of the reflectivity curve results in a > 50% reflectivity at 13.2 nm but < 15% reflectivity at 13.9 nm. As a result, the Cd laser is more advantageous for EUVL applications.

2. Experimental setup

The transient Nickel-like Cd laser pumped by a picosecond optical laser impinging at grazing incidence is described in detail in previous publications [1,8]. The pumping pulses are focused onto the target in a $30 \mu\text{m} \times 4 \text{ mm}$ FWHM line. The plasma is generated by exciting a polished Cd slab target with a sequence of an early prepulse of 15 mJ energy and 120 ps duration, followed after about 5 ns by a main prepulse of the same duration and ~350 mJ energy, which in turn is followed after a delay of 100 ps by an 8 ps duration, ~ 1 J energy heating pulse that is made to impinge at a grazing incidence angle of 23 degrees. Saturated operation is achieved with total pump energy as little as 1.4 J. The laser operates at a repetition rate of 5 Hz, and a 13.2 nm output pulse energy of up to 430 nJ [8]. The average power of the laser under typical operation conditions is $1 \mu\text{W}$.

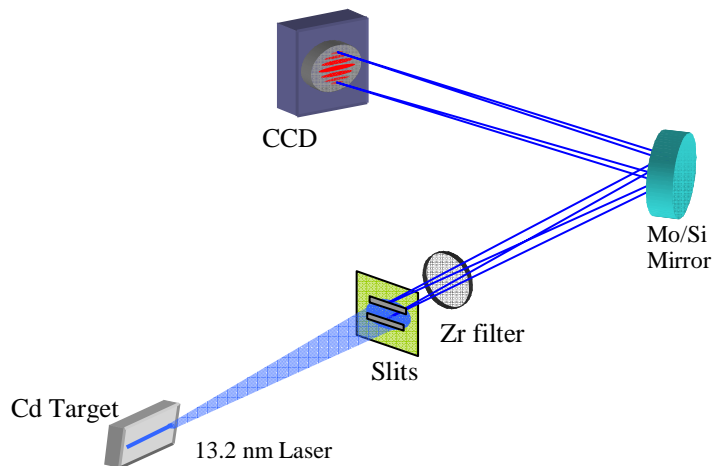


Fig. 1. Young's double-slit experiment setup for measuring the spatial coherence of a 13.2 nm soft x-ray laser.

The experimental setup of the coherence measurements is illustrated in Fig. 1. We used Young's double-slit interferometry to measure the degree of spatial coherence of the laser

beam. A set of slit pairs with separations of 30, 50, and 75 microns was used in the experiments. The width of each individual slit is 5 microns. The slits were placed at 105 mm from the laser target. A 0.2 μm thick self-supported Zr filter was used to block the Ti:sapphire laser and visible/ultraviolet radiations from the plasma. The 45-degree folding mirror is coated with Mo/Si multilayer, which has $\sim 50\%$ reflectivity at 13.2 nm and a spectral bandwidth of ~ 1 nm (FWHM). The interferograms were recorded with an EUV sensitive CCD camera having a back-illuminated 2048×2048 array of $13 \times 13 \mu\text{m}^2$ pixels. The total path length from the double-slit to CCD is 330 mm. The multilayer and Zr filters sufficiently prevent most unwanted wavelengths from reaching the CCD and allow us to record clean interferogram in a single shot. Given the fact that the 13.2 nm laser line has a linewidth of only about 0.001 nm, although it strongly dominates the spectrum, there is still a low level of background (typically 10% of the 13.2 nm radiation) in the CCD readouts originating from those EUV wavelengths falling into the 1-nm bandwidth of the multilayer. Assuming the background radiation from the plasma is isotropic, for each interferogram we recorded the background by moving the slit away from the soft x-ray laser beam path and repeated the shot under the same experimental condition. We then obtained a clean interferogram by subtracting the background from the original one. This process also automatically removes the uniform thermal dark current of the CCD.

3. Interferograms and interpretations

A typical interferogram recorded using a double slit with 30 μm separation is shown in Fig. 2(a). The double-slit was placed horizontally, in the direction perpendicular to the target, thus diffraction and interference pattern occurred in the vertical direction. We integrated the interferogram along both horizontal and vertical directions. The vertical one [Fig. 2(b)] can be seen as a lineout of the laser beam intensity profile, sampled by the slits. It provides useful information on beam size and divergence angle. The horizontally integrated one [Fig. 2(c)] is the overall double-slit interference pattern, from which an 'average' fringe visibility can be obtained. The high fringe visibility in Fig. 2(c) implies a high degree of spatial coherence for 30 μm separation.

A noticeable feature of the interferograms is the pronounced intensity irregularity, with many local intense spots in them. Those spots were observed in all the interferograms, regardless of slit orientation and Cd target length. Their peak intensities and positions changed randomly from shot to shot. Their presence causes complications on the analysis of the interferograms. For typical double-pinhole/slit coherence measurements, the relationship between fringe visibility V and the spatial coherence factor μ_{12} is [14]

$$V = \frac{2\sqrt{I_1 I_2}}{I_1 + I_2} |\mu_{12}| \quad \text{Eq. (1)}$$

where I_1 and I_2 are the beam intensities at the two individual slits. The fringe visibility V can be directly obtained from the interferogram as $V = (I_{\max} - I_{\min}) / (I_{\max} + I_{\min})$, where I_{\max} and I_{\min} are the intensity maxima and minima in the interferogram. Usually, the double-slit is positioned such that $I_1 \approx I_2$, which leads to the simple relationship $V = |\mu_{12}|$. However, in general cases when $I_1 \neq I_2$, Eq. (1) implies $V < |\mu_{12}|$, meaning measured fringe visibility would always underestimate the real degree of spatial coherence. As the difference between I_1 and I_2 becomes larger, the discrepancy between fringe visibility V and coherence factor will also become larger. In our experiments, the randomly located hot spots present in the beam microstructure make it practically impossible to position the slit so that $I_1 \approx I_2$ can be satisfied across the whole slit. The relative strength of I_1 and I_2 is also varying therefore the factor $2\sqrt{I_1 I_2} / (I_1 + I_2)$ can not be fully determined. The characteristic size of those spots at the double-slit plane, estimated by their sizes on the CCD and a simple geometric reduction, is around 100 μm . This is comparable to the slit separations used in the experiments. While two slits separated by 30 μm (the smallest separation used in experiments) may still sample those

$\sim 100 \mu\text{m}$ spots with roughly the same intensities, it is more likely that double-slits with $50 \mu\text{m}$ and $75 \mu\text{m}$ separations will see increasingly different intensities on individual slits. Such intensity difference will cause visibility variation even though $|\mu_{12}|$ could still be essentially constant.

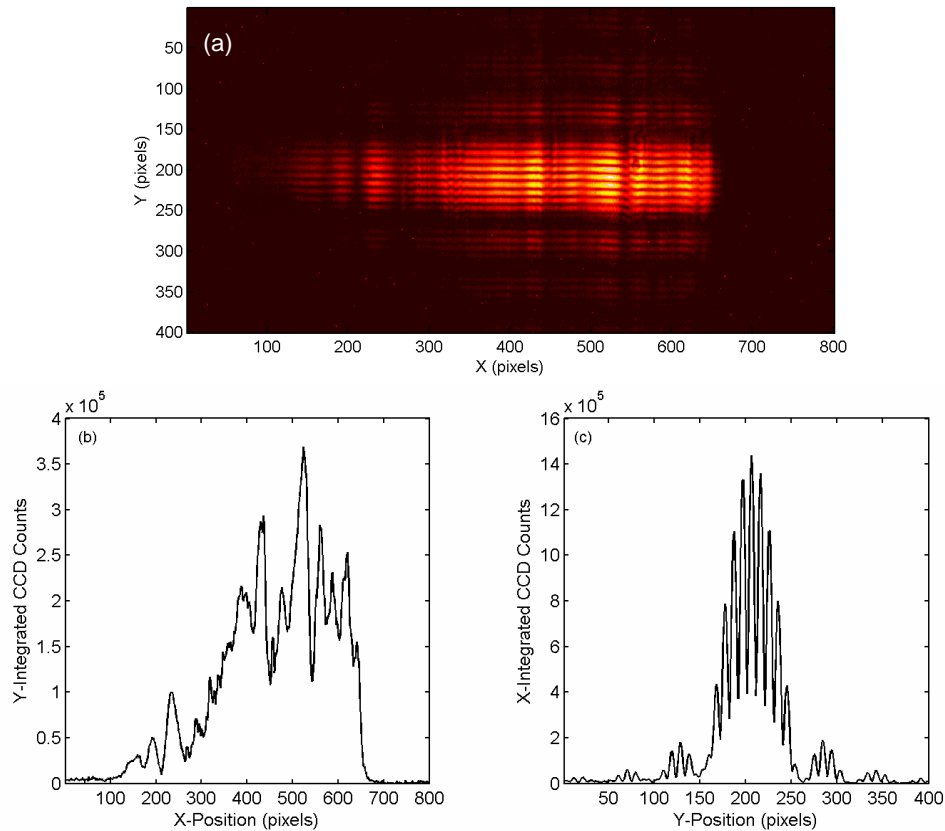


Fig. 2. (a) A typical two-slit interferogram recorded by the CCD for a $30 \mu\text{m}$ slit separation. The double-slit is placed horizontally (x-direction). (b) Integration of (a) in the vertical direction, which gives a lineout of the laser beam intensity profile. Intensity irregularities, or microstructures, are clearly observed. (c) Integration of (a) in the horizontal direction, which gives an 'average' interference pattern, whose fringe visibility is a measure of the spatial coherence.

We indeed observed fringe visibility variations in recorded interferograms. Figure 3 illustrates fringe patterns obtained using 4-mm-long target and horizontally placed (perpendicular to target surface) double-slits with separations of $30 \mu\text{m}$ (a), $50 \mu\text{m}$ (b), and $75 \mu\text{m}$ (c). For each separation, we first obtained an average fringe visibility (red lines) by integrating the whole interferogram, as described in earlier paragraph. We then manually scanned the interferogram along the slit orientation and picked a small region where the visibility is highest (blue lines in fig.). Consistent with the above discussions, the variation of fringe visibility with $30 \mu\text{m}$ double-slit is relatively small, where the best/average visibility is $0.69/0.59$. The visibility variation becomes larger with 50 and $75 \mu\text{m}$ double-slits, where best/average visibility is $0.52/0.23$ and $0.31/0.13$, respectively. Although we could not rule out the possibility that $|\mu_{12}|$ itself is varying in space, following the above discussion we believe the highest visibility observed is a more accurate representation of $|\mu_{12}|$, while the average visibility underestimates it.

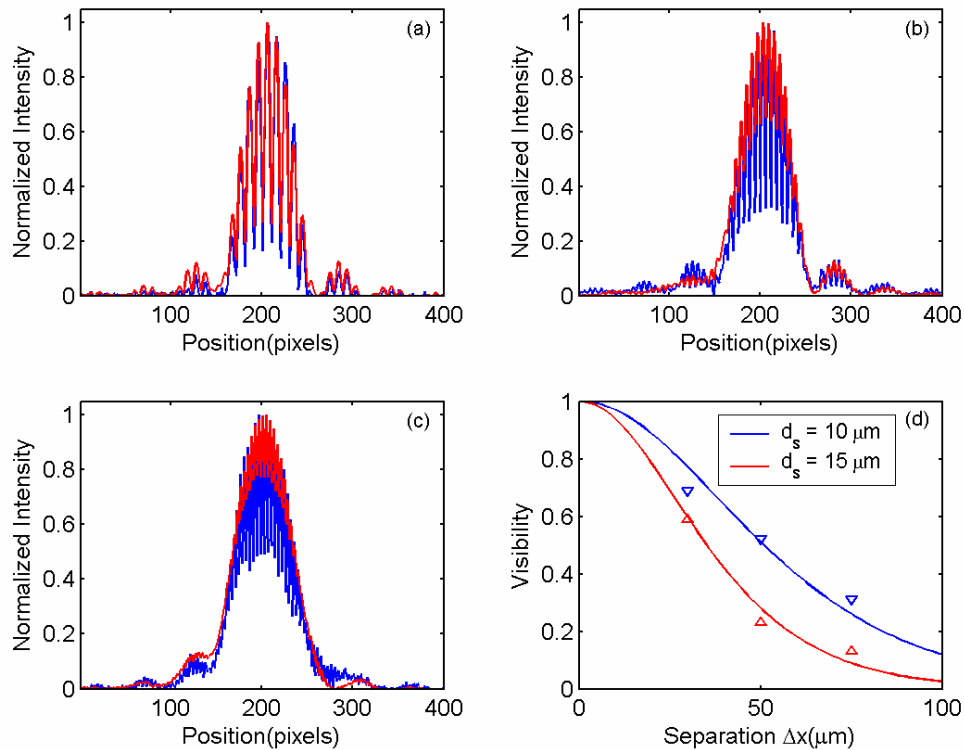


Fig. 3. (a)-(c). Interference fringes with average visibility (red), obtained by integrating the whole interferogram, and fringes with highest visibility (blue), picked by manually scanning the interferogram. For comparison the fringe patterns are normalized in intensity and overlap each other. The slit separations are (a) 30, (b) 50, and (c) 75 μm . (d) Experimental data (Δ, ∇) of fringe visibilities at different slit separations and theoretical predictions based on van Cittert-Zernike theorem. The source size is 10 μm [blue, corresponding to highest visibilities in (a-c)] and 15 μm (red, corresponding to average visibilities).

Having deduced values of $|\mu_{12}|$ for different separations, we can estimate the size of an equivalent incoherent source using van Cittert-Zernike theorem [14]. Assuming the source has a parabolic-like intensity profile of $I=I_0\cosh^{-2}(x/a)$ [15], to produce similar $|\mu_{12}|$ function at the double-slit plane, the source size (FWHM) is 10 μm (Fig. 3(d), blue curve). For comparison, using the average visibility data (red Δ) results in a source size of 15 μm FWHM (red curve). The above results are for horizontally placed slits; vertically placed slits (parallel to target plane) gave similar results. The spatial coherence properties seem to be the same in both directions.

For applications such as interferometry and coherent imaging, highly coherent radiation is needed. The laser has a very narrow linewidth ($\Delta\lambda/\lambda < 10^{-4}$), corresponding to a longitudinal coherence length of $\lambda^2/\Delta\lambda > 100 \mu\text{m}$, sufficient for most applications at this wavelength. To ensure high degree of spatial (transverse) coherence, adequate spatial filtering can be used [16]. Adopting the criteria set by ref. 14, we define a transverse coherence length at a given distance from the source as the distance L_c over which $|\mu_{12}(\Delta x)|$ drops to $\exp(-1/8) = 0.88$. From Fig. 3(d), L_c is 22 μm at the double-slit plane (105 mm from the source). Therefore, an angular filter with acceptance angle (2θ) of 0.4 mrad would provide radiation with very high degree of spatial coherence. We now estimate the throughput of such a spatial filter. The laser beam's divergence angle (FWHM) for the pumping conditions of this experiment, estimated from intensity profiles as in Fig. 2(c), is about 8 mrad in horizontal direction and 11 mrad in vertical direction. Comparing these numbers, the portion of the laser beam that can go through

the spatial filter is thus $(0.4\text{mrad})^2/(8\text{mrad}\cdot 11\text{mrad}) = 0.2\%$ of the total power. Notice that such coherent power is generated within a pulse duration of 5 ps [17], the laser's peak spectral brightness, a parameter closely related to a source's coherence properties and of particular value in imaging experiments, is $\sim 3 \times 10^{23}$ photons/sec/mm²/mrad² within less than 0.01% spectral bandwidth (based on 430 nJ pulse energy and a 15 μm laser exit diameter predicted by a hydrodynamic model), exceeding modern synchrotron radiation facilities at similar wavelengths.

The above results show that a good degree of spatial coherence exists on a lateral size roughly the same as those microstructures found in the intensity profile, but much smaller than the beam diameter. It has been recently suggested that these microstructures are the results of interference between many independent spatial modes when the EUV laser possesses good temporal coherence and short pulse duration [18, 19]. They could also be the results of those independent modes experiencing non-uniform gain inside the plasma and exiting the plasma at different angles due to refraction. These microstructures are important when using the laser as the illuminator in a microscope or in interferometry applications.

4. Spatial coherence versus plasma length

Based on amplified spontaneous emission (ASE), the improvement of spatial coherence of soft x-ray lasers largely depends on the formation of an elongated plasma column with large length-to-diameter ratio, for which the Fresnel number ($N_F = a^2/\lambda L$) is small. A small Fresnel number reduces the number of spatial modes that can get effective amplification inside the gain media (plasma), thus providing a practical mode selection mechanism [15, 20]. With even longer plasma length and strong refraction, refractive anti-guiding can further reduce the mode number and result in essentially full spatial coherence from a soft x-ray laser [21]. In our experiments, we compared interferograms recorded with same double-slits, but varying target lengths from 2 mm to 4 mm. As described in section 3, the interferograms contain information on beam intensity, divergence, and spatial coherence. With increasing target lengths, we observed increase of beam intensity, as expected. However, in the present experiment we did not observe noticeable improvement of spatial coherence with longer targets. As an example, Fig. 4 shows the comparison of two interferograms using a 50 μm separation double-slit, one recorded with 2 mm long target, the other 4 mm.

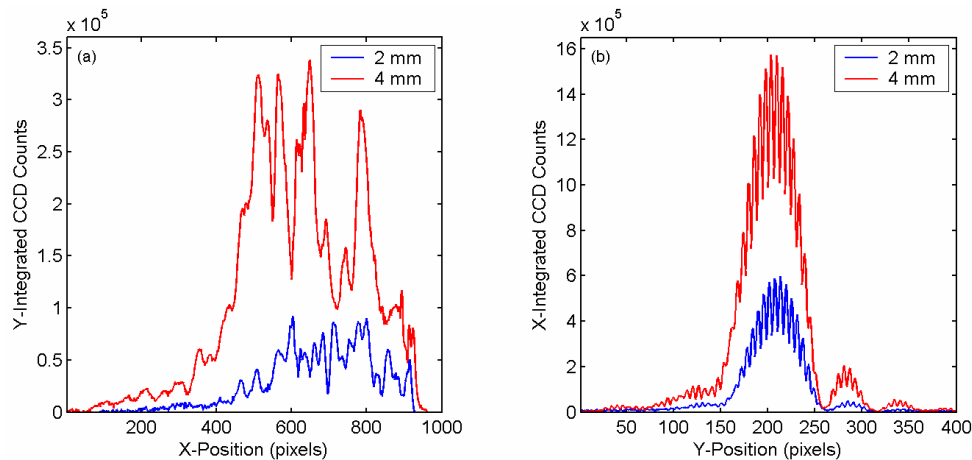


Fig. 4. Comparisons of beam intensity lineout (a) and integrated interference pattern (b) when the Cd target length is 2 mm (blue) and 4 mm (red). The CCD readouts are not normalized, thus providing a real comparison of beam intensity. There is no noticeable improvement of either spatial coherence, or beam quality when the target length is longer.

As shown in Fig. 4, the fringe visibility is essentially unchanged with longer target. Furthermore, the beam quality also showed limited improvement, with little change on the

divergence angle. If we treat the 4 mm plasma column as a 2 mm 'source' with another 2-mm long amplifier following it, the amplifier seems to amplify all spatial modes without preference. The lack of mode selection mechanism is an indication that the plasma lacks the high uniformity and cylindrical symmetry of the plasmas generated by fast capillary discharges, where rapidly improved spatial coherence is observed as a function of plasma column length [21]. Fluctuations in the plasma, such as "hose-type" random transverse displacements of the lasing medium, can also lead to decreased spatial coherence [22]. A more uniform plasma of longer length should allow for improved coherence. It can also be expected that a great improvement of the spatial coherence of this type of laser can be obtained by seeding the laser with a high coherence beam, possibly from another laser as in the double target setup [23], a cascaded amplifier setup with spatial filter in between, or a high-order harmonic source. In fact, a very recent experiment demonstrated that high harmonic seeding of a 32.6 nm wavelength Ne-like Ti soft x-ray laser amplifier pumped at grazing incidence achieved essentially full spatial coherence [24]. Such technique can yield compact high repetition rate soft x-ray lasers with full spatial and temporal coherence.

5. Summary

In summary, comprehensive spatial coherence measurements were performed for a 13.2 nm Cd laser pumped by grazing incidence. We observed significant microstructure in the beam intensity profile, whose influence on the coherence measurements is discussed. The transverse coherence length is found to be about 1/20 of the laser beam diameter.

Acknowledgments

We thank Mark Berrill (Colorado State University) for useful information on hydrodynamic simulation of the laser. This work was supported by the Engineering Research Centers Program of the National Science Foundation under NSF Award Number EEC-0310717.